Journal of The Electrochemical Society, **151** (7) C447-C454 (2004)
0013-4651/2004/151(7)/C447/8/$7.00 © The Electrochemical Society, Inc.

Electrodeposition of Al-Zr Alloys from Lewis Acidic Aluminum Chloride-1-Ethyl-3-methylimidazolium Chloride Melt

Tetsuya Tsuda,[a,*] Charles L. Hussey,[a,,z] Gery R. Stafford,[b,*] and Ole Kongstein[b]**

[a]*Department of Chemistry and Biochemistry, The University of Mississippi, University, Mississippi 38677, USA*
[b]*Materials Science and Engineering Laboratory, National Institute of Standards and Technology, Gaithersburg, Maryland 20899, USA*

The electrochemistry of Zr(IV) and Zr(II) and the electrodeposition of Al-Zr alloys were examined in the Lewis acidic 66.7-33.3 mol % aluminum chloride-1-ethyl-3-methylimidazolium chloride molten salt at 353 K. The electrochemical reduction of Zr(IV) to Zr(II) is complicated by the precipitation of $ZrCl_3$; however, solutions of Zr(II) can be prepared by reducing Zr(IV) with Al wire. Al-Zr alloys can be electrodeposited from plating baths containing either Zr(IV) or Zr(II), but for a given concentration and current density, baths containing Zr(IV) lead to Al-Zr alloys with the higher Zr content. This result was traced to the diminutive concentration-dependent diffusion coefficient for Zr(II). It was possible to prepare Al-Zr alloys containing up to ~17% atomic fraction (atom %) Zr. The structure of these deposits depended on the Zr content. Alloys containing less than 5 atom % Zr could be indexed to a disordered face-centered cubic structure similar to pure Al, whereas alloys containing ~17 atom % Zr were completely amorphous (metallic glass). The chloride pitting potentials of alloys with more than 8 atom % Zr were approximately +0.3 V relative to pure Al.
 [DOI: 10.1149/1.1753231]

Manuscript submitted October 28, 2003; revised manuscript received January 14, 2004. Available electronically May 19, 2004.

The maximum solubility of zirconium in face-centered cubic (fcc) aluminum is 0.08% atomic fraction (atom %). This occurs at the peritectic transformation point at 660.5°C. At room temperature, zirconium has negligible solubility in aluminum.[1] However like most aluminum-transition metal alloys, supersaturated solid solutions greatly exceeding the equilibrium solubility can be obtained by nonequilibrium processing methods. For example, solid solutions containing up to 3.0 atom % zirconium have been produced by rapid solidification[2-6] and vapor deposition.[7] The Al-Zr solid solution, although metastable, shows good thermal stability up to ~400-450°C. This observation is consistent with the general trend that the thermal stability of the solid solution is related to the melting point of the alloying addition; *i.e.*, the higher the melting point, the more stable the solid solution.[8] The thermal decomposition of the supersaturated solid solution results in the nucleation of a metastable Al_3Zr phase having an ordered cubic $L1_2$ structure (Cu_3Au-type)[5,6,9-13] and eventually the equilibrium Al_3Zr phase having a tetragonal structure. These two phases, cubic Al_3Zr and tetragonal Al_3Zr, have also been observed in supersaturated Al-Zr solid solutions produced by rapid quenching.[14]

The properties of aluminum and its alloys are significantly altered by the addition of zirconium. The rapid solidification of binary Al-Zr alloys with more than 0.15 atom % zirconium produces considerable grain refinement,[15,16] resulting in aluminum grain sizes typically less than 10 μm. The general explanation for this phenomenon is that $L1_2$ Al_3Zr acts as a low-energy nucleation site for fcc Al due to the similar crystal structures. Rapid quenching is required to ensure that the Al_3Zr solidifies with the metastable $L1_2$ structure rather than the equilibrium tetragonal structure. The presence of these fine Al_3Zr precipitates also raises the recrystallization temperature of aluminum, extending the good mechanical properties of the alloy to more elevated temperatures. Zirconium is also added to commercial high-strength aluminum alloys to improve toughness, stress-corrosion resistance, and quench sensitivity.[12,14] The addition of about 0.15 atom % Zr to several of the commercial aluminum alloys makes them superplastic due in part to the resulting grain refinement.[14,17-19] Typical elongations of 1000% can be consistently obtained with $Al_{97.6}Cu_{2.2}Zr_{0.2}$ alloys, whereas identically processed binary $Al_{97.4}Cu_{2.6}$ is comprised of large grains and has limited plasticity.

Although Al-Zr alloys with many interesting properties can be obtained by standard nonequilibrium processing methods as noted previously, the industrial application of these materials requires a processing method such as isothermal electrodeposition that can be used to produce alloy coatings of uniform thickness with reproducible composition and structure. A number of corrosion-resistant aluminum-transition metal alloys similar to Al-Zr have been electrodeposited from Lewis acidic chloroaluminate molten salts. These well-known melts are obtained by mixing a molar excess of anhydrous aluminum chloride with an appropriate chloride salt. Typical salts that have been used to prepare these melts include alkali chlorides such as NaCl or quaternary ammonium chloride salts such as 1-(1-butyl)pyridinium chloride or 1-ethyl-3-methylimidazolium chloride (EtMeImCl). Chloroaluminate molten salts have been used as baths for the electrodeposition of several corrosion-resistant aluminum-transition metal alloys; some examples of these alloys include Al-Cr,[20,21] Al-Mn,[22,23] Al-Ti,[24,25] and Al-V.[26] Progress in this area was recently reviewed.[27] Recently, Kawase and Ito[28] reported the electrodeposition of Zr and Al-Zr alloy films on carbon-coated ceramic substrates from solutions of electrogenerated Zr(II) in the LiCl-KCl eutectic molten salt at 823 K. Al(III) was the source of Al during the deposition of the Al-Zr alloys, and it was generated by the chemical oxidation of Al metal with Zr(II).

The electrochemistry of zirconium has been investigated in the Lewis acidic $AlCl_3$-NaCl melt.[29] In this study, insoluble green crystals of $ZrCl_3$ resulted from the electrochemical reduction of Zr(IV) in a melt containing 51-52 mol % $AlCl_3$ at 448 K. It was possible to reduce Zr(IV) to soluble Zr(III) in a very acidic melt (60 mol% $AlCl_3$) if the temperature was raised to 523 K or more, but the Zr(III) thus produced rapidly disproportionated to Zr(IV) and Zr(II). The precipitation of Zr(III) as $ZrCl_3$ was used to efficiently separate hafnium from zirconium in $AlCl_3$-NaCl melts of low acidity.[30] The electrochemistry of hexanuclear zirconium halide clusters was investigated in the $AlCl_3$-EtMeImCl melt containing 60 mol % $AlCl_3$.[31] However, no evidence for the electrodeposition of zirconium metal or Al-Zr alloy was obtained during this or any of the investigations just described. In this article, we report the electrodeposition of Al-Zr alloys on Cu substrates from the Lewis acidic $AlCl_3$-EtMeImCl molten salt and the electrochemistry of Zr(IV) and Zr(II) in this melt as it pertains to the electrodeposition of these alloys.

* Electrochemical Society Active Member.
** Electrochemical Society Fellow.
z E-mail: chclh@cheml.olemiss.edu

Experimental

Procedures used for the synthesis of EtMeImCl, purification of $AlCl_3$ by sublimation, and preparation and purification of the $AlCl_3$-EtMeImCl molten salt were identical to those described in a previous article.[26] Anhydrous $ZrCl_4$ (Aldrich, 99.9+%) was used as received. The preparation of the molten salt and all electrochemical experiments were carried out in a nitrogen gas-filled glove box (VAC Atmospheres Nexus system)[c] with O_2 and H_2O concentrations <5 ppm.

The UV-visible spectra of dissolved Zr ions were obtained by using a Varian Cary 5 spectrometer employing Wilmad no. 107-7 closed-type quartz cells. The path length of these cells was 0.10 cm.

Electrochemical experiments were conducted using an EG&G model 273 potentiostat/galvanostat controlled with EG&G PARC M270 software running on a Pentium III computer. Electronic resistance compensation was employed during all staircase voltammetry experiments. The step size used for staircase voltammetry, 2 mV, was small enough to permit the analysis of these resulting voltammograms with the conventional theories developed for linear scan voltammetry.[32]

A three-electrode Pyrex glass cell with a Teflon cap similar to that described in a previous article[33] was used for all experiments. A Pine Instruments Teflon-sheathed platinum rotating disk electrode (geometrical area 0.099 cm^2) was used as the working electrode during the voltammetry experiments. Coils of 0.10 cm diam aluminum wire (Alfa Aesar, 99.999%) were used for the counter and reference electrodes. These electrodes were immersed in pure melt with the same composition as the bulk melt, but were separated from the bulk melt by a porosity E glass frit (Ace Glass). The aluminum electrodes were cleaned with a mixture of concentrated aqueous H_2SO_4-HNO_3-H_3PO_4, rinsed with distilled H_2O, and dried under vacuum before use. All electrochemical experiments were carried out at 353 K unless otherwise noted.

The electrodeposition of Al-Zr alloys was performed with an EG&G PARC model 173 potentiostat/galvanostat equipped with a model 179 digital coulometer plug-in module. Alloy samples approximately 10 μm thick were deposited on a length of 1.25 mm diam copper wire (99.9% purity) from solutions of Zr(IV) or Zr(II) in the $AlCl_3$-EtMeImCl molten salt. The exposed surface area of the copper wire electrode was 0.80 cm^2. The wire was lightly sanded with emery cloth and then washed successively with distilled water and anhydrous ethanol. The copper wire was rotated at 2000 rpm during deposition. The electrodeposits were washed in distilled water and dried under vacuum in the glove box antechamber. The surface morphology of the electrodeposits was examined at NIST with scanning electron microscopy (SEM) by using a JEOL JXA-840 scanning electron microscope. The electrodeposits were also examined by X-ray diffraction (XRD) with a Siemens D-500 diffractometer employing Cu Kα radiation. The lattice parameters of the deposits were refined using the copper substrate reflections as an internal standard.

Potentiodynamic pitting corrosion measurements were carried out on these alloy samples at room temperature in deaerated, aqueous 0.1 mol L^{-1} solutions of NaCl. The reference electrode for these measurements was a sodium-saturated calomel electrode, and the counter electrode was a large surface area platinum wire coil. A known length of the plated Cu wire was exposed to the NaCl solution by using a heat-shrink tubing mask, and the sample was scanned at 0.5 mV s^{-1} by using linear staircase voltammetry with a step size of 2 mV.

Results and Discussion

Electrochemistry of $ZrCl_4$.—$ZrCl_4$ appeared to be very soluble in the melt. Figure 1 shows typical cyclic staircase voltammograms (CSVs) recorded at a stationary Pt disk electrode in the 66.7 mol % $AlCl_3$-EtMeImCl melt at 353 K before and after the addition of $ZrCl_4$. Before the addition of $ZrCl_4$, the only waves appearing in the voltammogram are those due to the deposition and stripping of aluminum according to the following well-known reaction

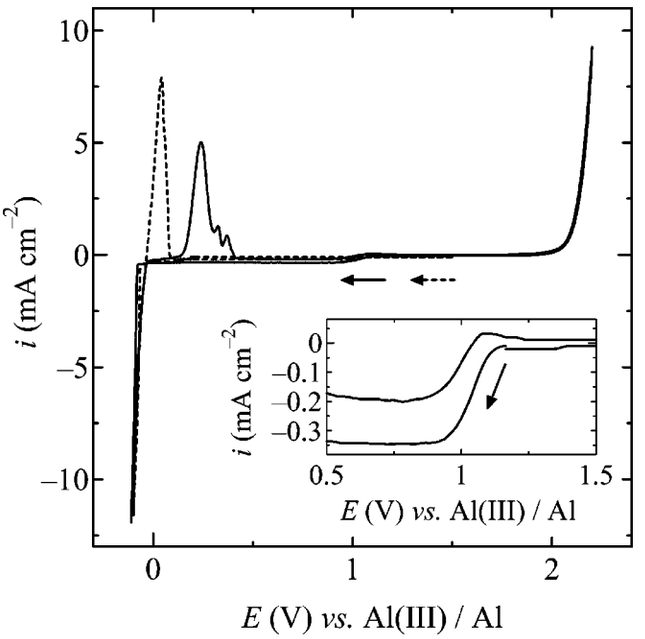

Figure 1. CSVs recorded at a platinum stationary disk electrode in the 66.7-33.3 mol % $AlCl_3$-EtMeImCl melt: (——) 19.5 mmol L^{-1} $ZrCl_4$; (— — —) pure melt. Inset: magnified region of the CSV recorded in melt containing $ZrCl_4$. The sweep rate was 10 mV s^{-1}, and the step size was 2 mV.

$$4Al_2Cl_7^- + 3e^- \rightleftharpoons Al + 7AlCl_4^- \quad [1]$$

After the dissolution of $ZrCl_4$, a small, ill-defined reduction wave with a peak potential, E_{pc}, of about 0.92 V was also apparent (see Fig. 1 inset). In addition, the wave ascribed to the reduction reaction in Reaction 1 shows a small negative shift, the oxidation wave due to the stripping of the pure Al deposit from the Pt electrode in pure melt is absent, and new stripping waves are evident at more positive potentials. The latter stripping waves are attributed to the oxidation of one or more electrodeposited Al-Zr alloy phases that are more stable toward oxidation than pure Al. The electrodeposition of Al-Zr alloys from these solutions is discussed in a later section.

The voltammetric wave at $E_{pc} \sim 0.92$ V is shown in more detail in Fig. 2. It was difficult to obtain reproducible results for this wave. In many cases, it was only possible to obtain a well-defined wave by polishing the platinum electrode surface before each scan. The difference in the peak potential and half-peak potential, $E_{pc} - E_{pc/2}$, for this wave varied between 0.08 and 0.12 V and did not display any obvious dependence on the scan rate over the range extending from 0.005 to 0.500 V s^{-1}. The smaller values of $E_{pc} - E_{pc/2}$ are reasonably close to the theoretical value of 0.07 V for a one-electron reversible reaction at 353 K, leading us to conclude that the reduction wave in Fig. 2 corresponds to the Zr(IV)/Zr(III) electrode reaction. If the voltammetric scan is reversed immediately after the reduction wave at 0.92 V and scan rates greater than 50 mV s^{-1} are employed, then an associated oxidation wave is observed at $E_{pa} \sim 1.09$ V. Experiments conducted at a fixed scan rate revealed that the voltammetric peak reduction current, i_{pc}, for the wave at 0.92 V did not always display a linear dependence on the $ZrCl_4$ concentration. This behavior was most pronounced at high $ZrCl_4$ concentrations and slow scan rates, and it was traced to the formation of a

[c] Certain trade names are mentioned for experimental information only; in no case does it imply a recommendation or endorsement by the National Institute of Standards and Technology (NIST).

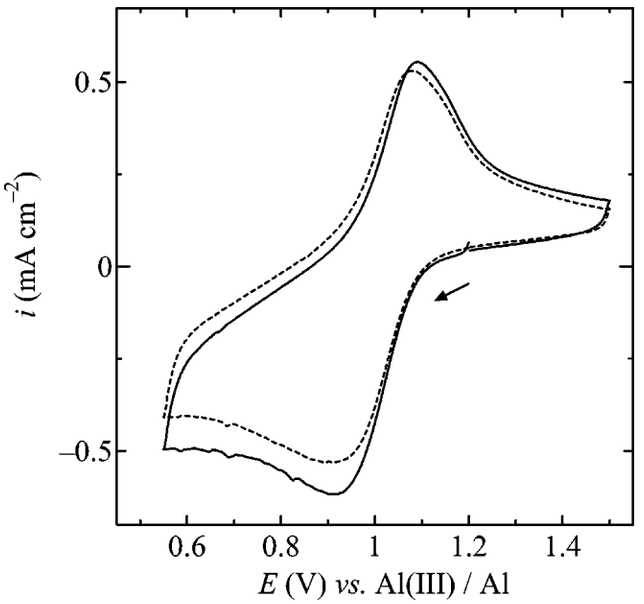

Figure 2. CSVs recorded at a platinum stationary disk electrode in the 66.7-33.3 mol % $AlCl_3$-EtMeImCl melt containing 11.6 mmol L^{-1} $ZrCl_4$: (——) first scan and (- - - -) fifth scan by continuous voltammetry. The sweep rate was 100 mV s^{-1}, and the step size was 2 mV.

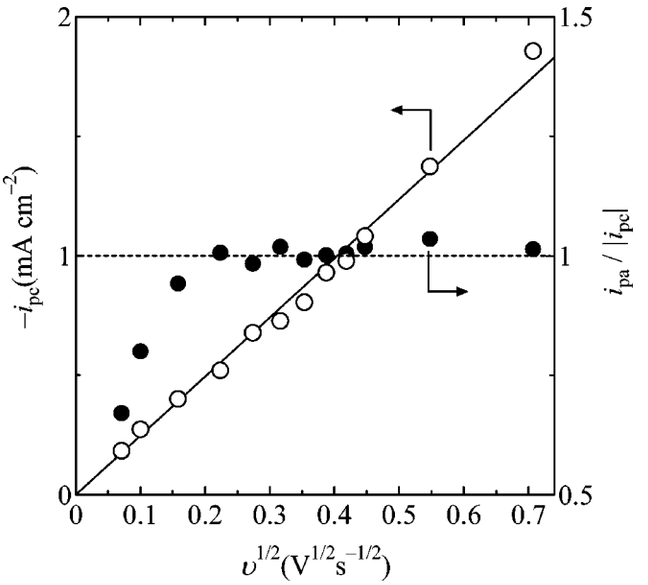

Figure 3. Peak reduction current density and ratio of the anodic-to-cathodic peak currents as a function of sweep rate for a series of voltammograms similar to that shown in Fig. 2.

surface film on the electrode during the reduction of Zr(IV). This film led to a decrease in the active area of the electrode and to many of the other anomalous results that were obtained for this voltammetric wave.

The reduction of Zr(IV) was also examined as a function of scan rate at a fixed concentration. Figure 3 shows a plot of the peak reduction current, i_{pc}, *vs.* the square root of the scan rate, $\upsilon^{1/2}$. Each data point in this figure is the average of several measurements. The linearity of this plot indicates that the reduction of Zr(IV) is a diffusion-controlled process. An estimate of the peak current ratio, $i_{pa}/|i_{pc}|$ was obtained by using Nicholson's semiempirical method.[34] This ratio is less than one at very slow scan rates, but increases to one at faster scan rates (Fig. 3). This latter result suggests that an irreversible homogeneous following chemical step is coupled to the electron-transfer reaction.[35] Because $ZrCl_3$, but not $ZrCl_2$, is insoluble in Lewis acidic chloroaluminate melts and in molten $AlCl_3$, this coupled chemical step must be due to the precipitation of $ZrCl_3$, as was found during the reduction of Zr(IV) in Lewis acidic $AlCl_3$-NaCl.[29] Thus, the reduction wave at *ca.* 0.92 V most likely involves the following sequence of reactions

$$Zr(IV)(solv) + e^- \rightleftharpoons Zr(III)(solv) \quad [2]$$

$$Zr(III)(solv) + 6AlCl_4^- \rightarrow ZrCl_3(s) + 3Al_2Cl_7^- \quad [3]$$

The latter reaction is the source of the passivating film that forms on the electrode surface at slow scan rates or high Zr(IV) concentrations. We also attempted to investigate the Zr(IV)/Zr(III) reaction by carrying out controlled potential reduction at a large surface area platinum screen electrode at an applied potential of 0.80 V. After the passage of a fraction of the charge necessary to reduce all of the Zr(IV), the electrode became completely passivated by the aforementioned surface film, and the solution became cloudy from a precipitate.

The diffusion coefficient for Zr(IV), $D_{Zr(IV)}$, and the Stokes-Einstein product, $D_{Zr(IV)}\eta/T$, where η is the absolute viscosity of the molten salt, were calculated from the data in Fig. 3. The viscosity data taken from Fannin *et al.*[36] were used for the latter calculation. The diffusion coefficient for the related group IV species, Ti(IV), that was measured in the 60.0 mol % melt at 300 K is given in Table I for comparison. $D_{Ti(IV)}$ can be compared to $D_{Zr(IV)}$ through the Stokes-Einstein product, $D\eta/T$, which considers both the temperature of the measurement and the absolute viscosity of the solvent. $D\eta/T$ is a relative measure of the solvodynamic radius of the diffusing species.[37] A comparison of the calculated Stokes-Einstein products given in Table I shows that, despite the seemingly large differences in $D_{Zr(IV)}$ and $D_{Ti(IV)}$, the two group IV species have roughly comparable solvodynamic radii. The somewhat smaller value of $D_{Ti(IV)}\eta/T$ may simply reflect the fact that Ti(IV) vaporizes rapidly from the melt as $TiCl_4$.[25] Thus, the diffusion coefficient data reported in the literature for Ti(IV) may have been

Table I. Summary of electrochemical data for titanium and zirconium solutes in Lewis acidic $AlCl_3$-EtMeImCl.

	Method	Temperature (K)	mol % $AlCl_3$	Concentration (mmol L^{-1})	$10^7 D$ (cm^2 s^{-1})	$10^{11}\eta D/T$ (g cm s^{-2} K^{-1})	Reference
Ti(IV)	NPV	300	60.0	40.0	8.1	39	38
Zr(IV)	CV	353	66.7	4.85	42	58	This work
Ti(II)	RDE-CV	353	66.7	12.6	2.2	3.1	25
	RDE-CV	353	66.7	25.2	1.2	1.6	25
Zr(II)	RDE-CV	353	66.7	5.40	1.2	1.7	This work
	RDE-CV	353	66.7	19.5	0.64	0.88	This work

NPV: Normal pulse voltammetry, CV: cyclic voltammetry, RDE-CV: cyclic voltammetry using a rotating Pt disk electrode.

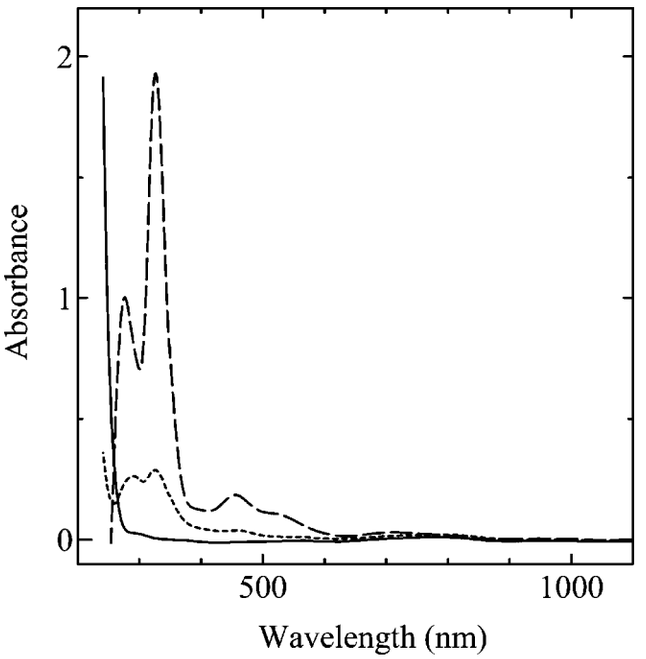

Figure 4. UV-visible spectra of the 66.7-33.3 mol % $AlCl_3$-EtMeImCl melt containing 5.04 mmol L^{-1} $ZrCl_4$ (——) before and (— — —) after reduction of the Zr(IV) with Al metal and (- - - -) with Zr metal.

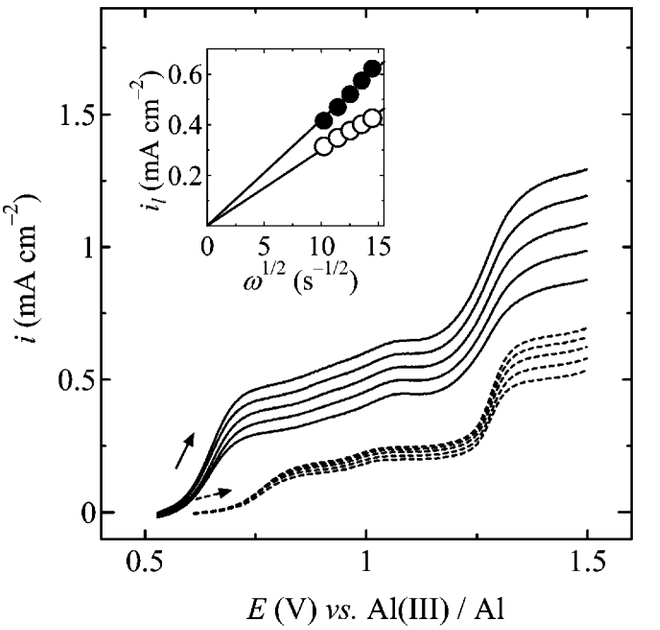

Figure 5. LSVs recorded at a Pt-RDE in the 66.7-33.3 mol % $AlCl_3$-EtMeImCl melt containing (——) 19.5 and (- - - -) 5.40 mmol L^{-1} Zr(II). The sweep rate was 10 mV s^{-1}; the rotation rates were 1000, 1250, 1500, 1750, and 2000 rpm; and the step size was 2 mV. (Inset) Relationship between the limiting current densities and the square root of the angular frequency of rotation: (●) 19.5 mmol L^{-1} Zr(II), 0.80 V and (○) 5.40 mmol L^{-1} Zr(II), 0.90 V.

measured under conditions that did not take into account the vaporization loss of $TiCl_4$, which would lead to smaller values of $D_{Ti(IV)}$ and $D_{Ti(IV)}\eta/T$.

Overall, these electrochemical results are very similar to those obtained during an investigation of the related titanium system in this same molten salt.[38] In this case, the Ti(IV)/Ti(III) reaction was also complicated by a coupled irreversible following chemical reaction involving precipitation of the trivalent chloride, $TiCl_3$.[38] The insolubility of $TiCl_3$ was also noted during previous investigations involving the electrodeposition of Al-Ti alloys from the Lewis acidic $AlCl_3$-EtMeImCl and $AlCl_3$-NaCl molten salts.[24,25,39] A recent investigation of the related vanadium system indicated that VCl_3 was virtually insoluble in the Lewis acidic $AlCl_3$-EtMeImCl melt, whereas the divalent species, VCl_2, was soluble.[26] Thus, the insolubility of the groups IV and V trivalent chlorides appears to be a general trend in Lewis acidic chloroaluminate melts.

Chemical Reduction of $ZrCl_4$.—The CSV recorded for the solution containing Zr(IV) shown in Fig. 1 does not exhibit any obvious wave for the reduction of Zr(III) to a lower oxidation state species, even at fast scan rates where the coupled chemical step is unimportant. However, as we show, compact, chloride-free deposits containing Zr metal can be obtained by the electrochemical reduction of Zr(IV). This indicates that Zr(III), irrespective of its chemical or physical form, must eventually undergo reduction as the potential approaches 0 V *vs.* Al(III)/Al. Therefore, we carried out a series of experiments to determine if it is possible to obtain Zr(II) by the chemical reduction of Zr(IV). There is considerable evidence for the existence of this species. For example, Ruff and Wallstein[40] reported that Zr(II) can be obtained by the chemical reduction of molten $ZrCl_4$ with Al. Larsen *et al.*[41] obtained the characteristic green crystals of $ZrCl_3$ by the reduction of $ZrCl_4$ dissolved in molten Al_2Cl_6 with Al or Zr metal at 503-583 K. However, the resulting $ZrCl_3$ is unstable in molten Al_2Cl_6 and slowly disproportionates to an insoluble brown-colored Zr(II) species, $(ZrCl_2)_2AlCl_3$, and $ZrCl_4$. Based on previous work with the related V(II) and Ti(II) species,[25,26] we expect Zr(II) to be stable and soluble in the acidic $AlCl_3$-EtMeImCl melt.

Figure 4 shows UV-vis spectra of a solution of Zr(IV) in the 66.7 mol % melt before and after this solution was stirred with Al metal at 353.2 K for 3 days. During the reaction between Zr(IV) and Al, the solution changed from colorless to reddish-brown with no evidence of the formation of the green precipitate of $ZrCl_3$ reported by Larsen *et al.*[41] in molten Al_2Cl_6 and by Gilbert *et al.*[29] in acidic $AlCl_3$-NaCl. We ascribe this soluble reddish-brown reduction product to a Zr(II) species; this assignment is supported by the electrochemical experiments described in a later section. When we repeated these experiments in the 60.0 mol % melt containing approximately the same initial concentration of Zr(IV), we obtained a different result. Under the less acidic conditions of this melt, the reduction of Zr(IV) by Al also results in a reddish-brown solution, but the visual density of the color and the intensity of the absorption bands in the spectrum of this solution are greatly diminished compared to the solution resulting from similar experiments in the 66.7 mol % melt. In addition, the reaction vessel contained a considerable quantity of the green crystals of $ZrCl_3$. Likewise, when we repeated these experiments with Zr(IV) in the 66.7 mol % melt by using Zr metal as the reducing agent, the green precipitate of $ZrCl_3$ was obtained in abundance and only a small amount of Zr(II) was obtained. Thus, it appears that Zr(IV) can only be completely reduced to Zr(II) by using Al metal and employing the very acidic 66.7 mol % melt (Fig. 4).

During the chemical reduction of Zr(IV) with Al in the 66.7 mol % melt described previously, the rest potential of a Pt-RDE electrode immersed in the solution shifted to a value considerably negative of the Zr(IV)/Zr(III) couple. Figure 5 shows a series of CSVs that were recorded at a Pt-RDE at different rotation rates in two solutions that were prepared in this melt by the chemical reduction of Zr(IV) with Al metal. The concentrations of Zr(IV) used to prepare these two solutions were different, and the CSVs were initiated

from the rest potential of each solution. Each of the CSVs in Fig. 5 shows two well-defined oxidation waves, and plots of E *vs.* $\log[(i - i_1)/i]$ were linear for both waves. Analysis of the intercepts of these plots gave half-wave potentials, $E_{1/2}$, of 0.80 ± 0.01 and 1.29 ± 0.01 V for the first and second waves, respectively, in the CSVs recorded in the 5.40 mM solution, and $E_{1/2}$ = 0.66 ± 0.00 and 1.28 ± 0.00 V, respectively, for the oxidation waves acquired in the 19.5 mM solution. Thus, $E_{1/2}$ for the first oxidation wave, but not the second wave, in these CSVs displays a dependence on the concentration of the electroactive species. Calculations based on the slopes of these plots yielded n = 0.9 ± 0.1 and 1.0 ± 0.2 for the first and second waves, respectively, indicating that both waves correspond to one-electron reactions. Overall, the CSVs in Fig. 5 are very similar in appearance to those recorded during the oxidation of Ti(II) in this same melt.[25] Taken together, these observations provide good evidence that the species produced during the chemical reduction of Zr(IV) with Al is Zr(II). The maximum concentration of Zr(II) that could be obtained by the Al reduction of Zr(IV) was about 19 mmol L^{-1}.

The inset of Fig. 5 shows that the limiting current densities for the first oxidation waves in Fig. 5 obey the Levich relationship. The diffusion coefficients and Stokes-Einstein products that were calculated from these limiting current density data are collected in Table I along with values for $D_{Ti(II)}$ and $\eta D_{Ti(II)}/T$. Generally, the values of $D_{Zr(II)}$ are in reasonable agreement with those for $D_{Ti(II)}$ in this same molten salt. However, like $D_{Ti(II)}$, $D_{Zr(II)}$ varies with the concentration of the electroactive solute, becoming smaller as the solute concentration increases. For Ti(II), this phenomenon is attributed to polymerization of the Ti(II) species as $[Ti(AlCl_4)_2]_m$, with m increasing as the Ti(II) concentration is increased.[25,39,42,43] Given the overall similarity of the chemistry of Ti(II) and Zr(II), polymerization of Zr(II) is also expected. The observed concentration dependence of $E_{1/2}$ for the first Zr(II) oxidation waves, but not the second waves, in Fig. 5 may also be related to such a phenomenon. However, additional experiments beyond the scope of this investigation are required to fully characterize the complicated electrochemistry of Zr(IV) and Zr(II) in the Lewis acidic $AlCl_3$-EtMeImCl melt.

Electrodeposition of Al-Zr alloys.—The electrodeposition of bulk Al-Zr alloys was examined by using dc galvanostatic methods at 353 K in the 66.7 mol % melt containing either Zr(IV) or Zr(II) prepared by the Al reduction of Zr(IV) (*vide supra*). Because there are no side reactions to compete with the Al-Zr deposition process, the current efficiency is nearly 100%. The substrate for these deposition experiments was a copper rotating wire electrode. A rotation rate of 2000 rpm was used for these experiments to be consistent with previous studies involving the electrodeposition of Al-Ti[25] and Al-V[26] from this same molten salt. The compositions of the Al-Zr alloys resulting from these experiments are shown as a function of current density in Fig. 6. The data in this figure lead to two conclusions. First, the Zr content of the electrodeposited alloys decreases with increasing current density. Second, solutions of Zr(IV) lead to Al-Zr alloys containing greater amounts of Zr than Zr(II) solutions of equal concentration.

The first result is expected because at low reduction current densities and correspondingly less negative potentials, the partial current density for Zr would be a larger fraction of the total current. As the current density is increased, the partial current for the reduction of the Zr species should reach a limiting value, whereas the partial current for the reduction of $Al_2Cl_7^-$, which is present in this melt at a concentration of 3.24 M at 353 K, continues to increase. This behavior is a common feature of overpotential alloy deposition in chloroaluminate melts and was observed during the electrodeposition of Al-Cr[20,21] Al-Mn,[23,44] Al-Mo,[45] and Al-Ti.[24,25,39,46] The finding that plating solutions containing Zr(IV) lead to alloys with higher Zr content than plating solutions containing equal concentrations of Zr(II) may be reconciled by considering the diffusion coefficient data in Table I. Because the concentration-dependent diffusion coefficient for Zr(II) is only a small fraction of that for Zr(IV), the observed inefficiency of Zr(II) for plating Al-Zr alloys must be directly related to the mass-transport limitations imposed by the diminutive diffusion coefficient of the latter species.

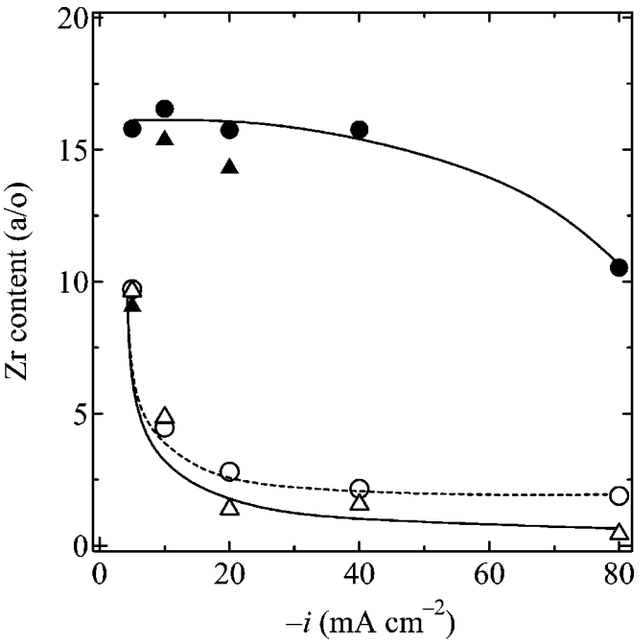

Figure 6. Relationship between the applied current density and Zr content of Al-Zr deposits prepared in the 66.7-33.3 mol % $AlCl_3$-EtMeImCl melt: (●) 19.5 mmol L^{-1} Zr(IV), (○) 19.5 mmol L^{-1} Zr(II), (▲) 4.85 mmol L^{-1} Zr(IV), and (△) 4.85 mmol L^{-1} Zr(II). The electrode rotation rate was 2000 rpm.

Characterization of electrodeposited Al-Zr alloys.—The surface morphology of Al-Zr deposits of varying composition is shown in Fig. 7. The 1.4 atom % Zr deposit, Fig. 7a, is nodular and the nodules tend to follow the defects, *i.e.*, striations, that were introduced into the drawn wire substrate as the result of its processing. The nodules are typically 5-10 μm diam and appear to be single crystals. The 4.9 atom % Zr deposit, Fig. 7b, shows significant grain refinement. The nodules are typically 1 μm diam or less. Although the 4.9 atom % Zr deposit was made at a lower current density than the 1.4 atom % Zr deposit, it has a smaller nodule size, suggesting that the grain refinement is driven by the incorporation of Zr into the alloy rather than the deposition overpotential. Similar behavior was recently reported for electrodeposited Al-Ti alloys.[25] The deposit morphology changes significantly with further additions of Zr. Figure 7c shows the surface of a 15.9 atom % Zr deposit with the compact, rounded nodular structure that is generally associated with metallic glasses.

Electrodeposits containing 1.4-16.6 atom % Zr were examined by XRD. The diffraction patterns for selected deposits are shown in Fig. 8. Deposits containing less than 5 atom % Zr have diffraction patterns that can be indexed to a chemically disordered fcc structure very similar to that of pure aluminum, indicating that the Al-Zr alloy is a single phase, supersaturated solid solution. The lack of 100 and 110 superlattice reflections at 21.9° and 31.2°, respectively, indicates that the alloy does not exhibit Ll_2 ordering. These patterns indicate that the Al grains are randomly oriented and have no preferred crystallographic texture. Two distinct changes in the diffraction patterns with increased Zr composition are observed. The first is a shift in the reflections to lower values of 2θ. This is to be expected as the larger Zr atoms (lattice volume of 23.3 Å^3 atom^{-1}) substitute for Al (lattice volume of 16.6 Å^3 atom^{-1}) in the fcc lattice. The second change is the development of a broad reflection centered around a 2θ of about

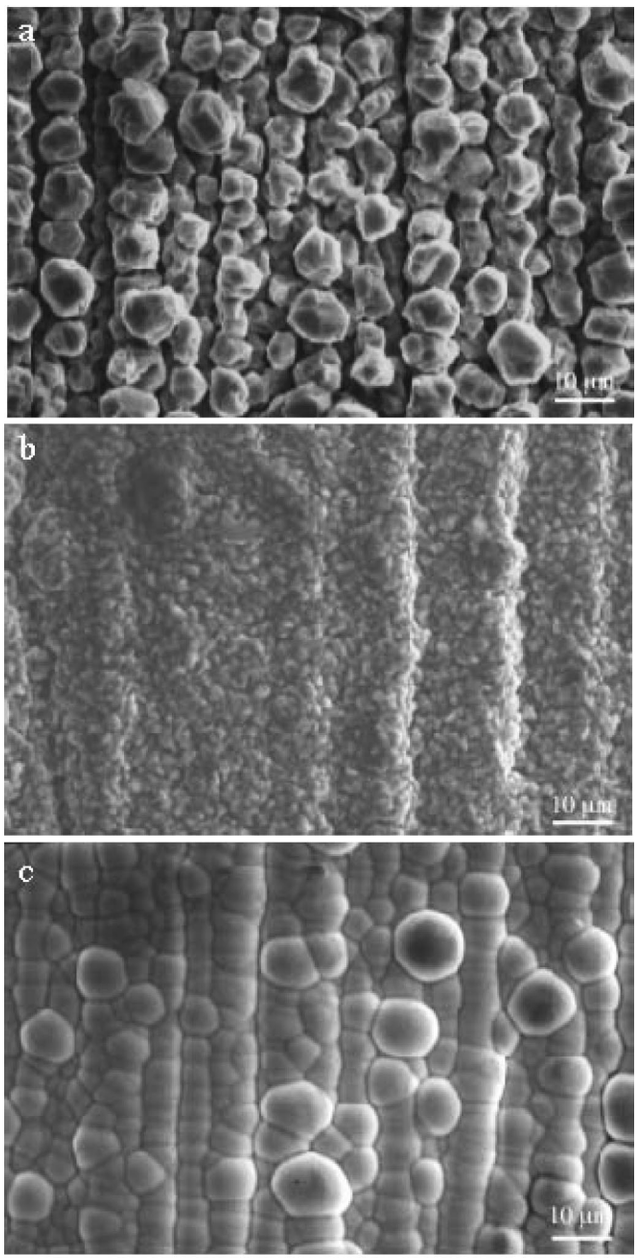

Figure 7. SEM micrographs of Al-Zr alloys electrodeposited from the 66.7-33.3 mol % $AlCl_3$-EtMeImCl melt: (a) 1.4 atom % Zr, 20 mA cm^{-2}, 4.85 mmol L^{-1} Zr(IV); (b) 4.9 atom % Zr, 10 mA cm^{-2}, 4.85 mmol L^{-1} Zr(IV); and (c) 15.9 atom % Zr, 20 mA cm^{-2}, 10.2 mmol L^{-1} Zr(IV).

39°. The deposit containing 9.7 atom % Zr appears to be comprised of an amorphous phase in addition to fcc Al, whereas the deposit containing 16.6 atom % Zr is completely amorphous.

The lattice parameters of the fcc Al phase were refined by using the copper substrate reflections as an internal standard. These parameters are plotted as a function of alloy composition in Fig. 9. In addition, literature values for single phase solid solutions produced by rapid solidification are plotted for comparison.[2,4] As-quenched alloys containing more that 3.0 atom % Zr were noted to be two-phase.[4] Similar levels of supersaturation have been produced by vapor deposition.[7] Clearly, solid solutions containing up to about 2 atom % Zr follow Vegard's law; *i.e.*, the lattice volumes of the solid solution are simply linear combinations of the constituent lattice

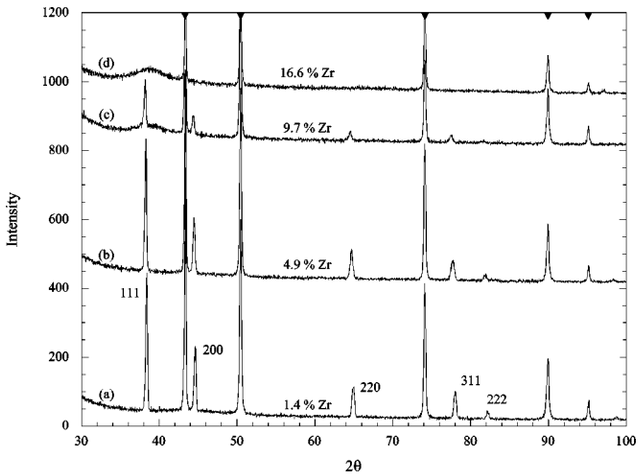

Figure 8. XRD patterns (Cu Kα) from as-deposited Al-Zr alloys containing (a) 1.4, (b) 4.9, (c) 9.7, and (d) 16.6 atom % Zr. Copper reflections from the substrate are denoted by ▼ at the top of the figure.

volumes. In the region of 2-5 atom % Zr, the lattice volumes are smaller than those predicted by Vegard's law. It appears that this deviation is real because there is no evidence for any second phase in either the rapidly solidified[4] or electrodeposited material in this composition range, *e.g.*, see Fig. 8b. The highest degree of supersaturation was observed in deposits nominally containing 8-10 atom % Zr. SEM examination of these deposits indicated that the Zr was not homogeneously distributed throughout the deposit. Energy-dispersive spectroscopy clearly showed regions containing high levels of Zr with a surface morphology similar to Fig. 7c and regions containing low levels of Zr that had a surface morphology similar to Fig. 7b. In certain areas, a supersaturated fcc phase nucleated on top of a Zr-rich amorphous layer, suggesting that insufficient Zr was available to maintain deposition of the amorphous phase. Because the Zr is partitioned between the fcc and amorphous phases in these two-phase deposits, the actual amount of Zr retained in solid solution can be estimated from the lattice parameter to be about 6 atom % in these electrodeposits. This level of supersaturation is at least twice that observed in vapor deposited or rapidly quenched alloys reported to date.

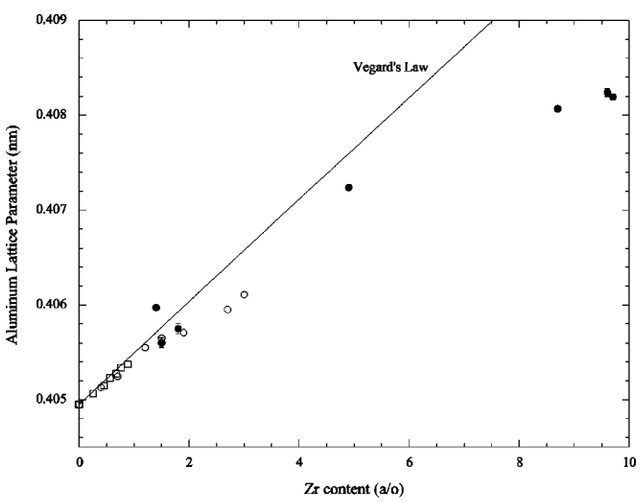

Figure 9. Lattice parameters for fcc Al as a function of Al-Zr alloy composition: (●) this work, (□) Burov and Yakunin,[2] (○) Sahin and Jones,[4] and (——) Vegard's law.

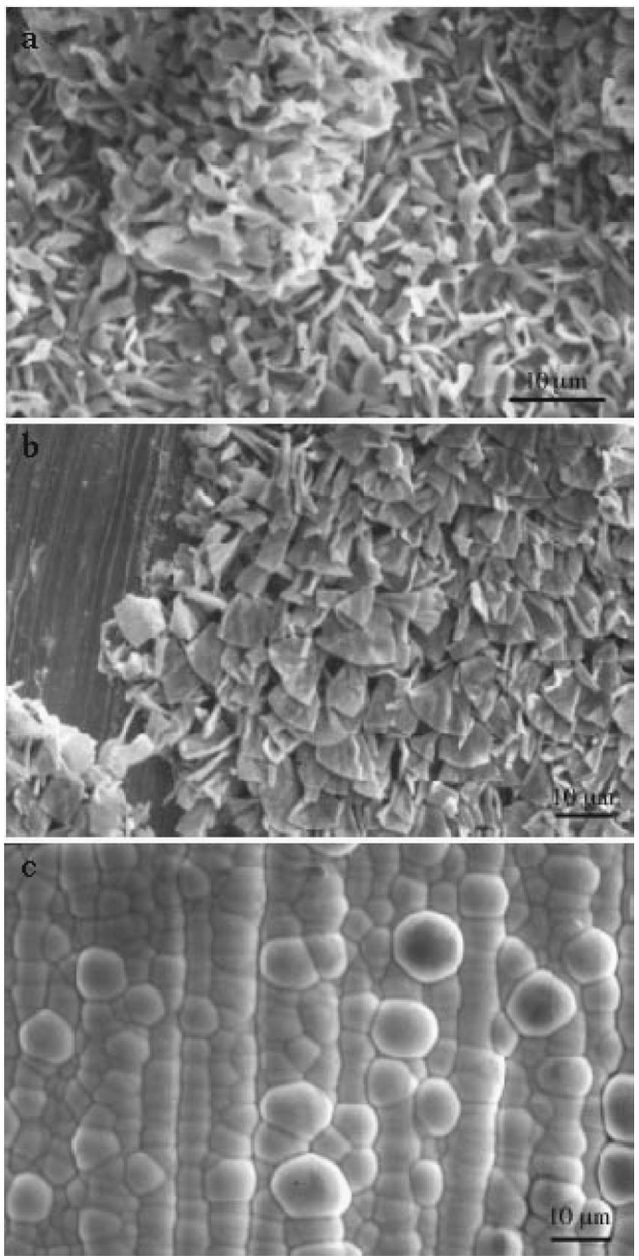

Figure 10. SEM micrographs of Al-Zr alloys electrodeposited from 66.7-33.3 mol % $AlCl_3$-EtMeImCl melt: (a) 15.6 atom % Zr, 5 mA cm^{-2}, 19.5 mmol L^{-1} Zr(IV); (b) 16.6 atom % Zr, 10 mA cm^{-2}, 19.5 mmol L^{-1} Zr(IV); and (c) 15.9 atom % Zr, 20 mA cm^{-2}, 10.2 mmol L^{-1} Zr(IV).

Two-phase regions are often observed in electrodeposited aluminum-transition metal alloys when the concentration of the transition metal exceeds the limit of supersaturation in the fcc Al solid solution. The appearance of the second phase, which often has an amorphous structure, generally causes a relaxation in the supersaturation of the solid solution. This has been observed in Al-Cr[20] and Al-Mn[47] alloys electrodeposited from $AlCl_3$-NaCl electrolytes. The two-phase region observed in electrodeposited Al-Zr is clearly different from that reported in alloys deposited from the high-temperature melt. We have not observed the fine-grained duplex structure that is typically observed in homogeneous two-phase alloys, nor have we observed a relaxation in the supersaturation of Zr in the fcc phase when the amorphous phase is present. This suggests

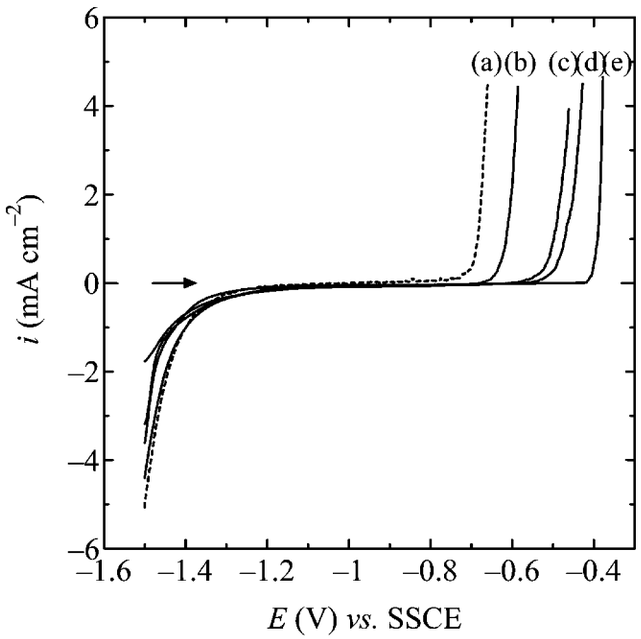

Figure 11. Anodic polarization curves recorded in deaerated 0.1 mol L^{-1} aqueous NaCl for Al-Zr alloys electrodeposited from the 66.7-33.3 mol % $AlCl_3$-EtMeImCl melt: (a) Al (99.999%), (b) $Al_{97.8}Zr_{2.2}$, (c) $Al_{97.2}Zr_{2.8}$, (d) $Al_{95.5}Zr_{4.5}$, and (e) $Al_{84.3}Zr_{15.7}$. The sweep rate was 0.5 mV s^{-1}, the step size was 2 mV, and the experiments were conducted at room temperature.

that the two-phase Al-Zr deposits are not intimately co-deposited but consist of large, discrete regions of single phase material. The nonuniform distribution of Zr and the resultant inhomogeneous surface morphology revealed by SEM are consistent with this conclusion. The phase distribution appears to follow a composition distribution that seems to be the result of a nonuniform current distribution along the copper wire electrode.

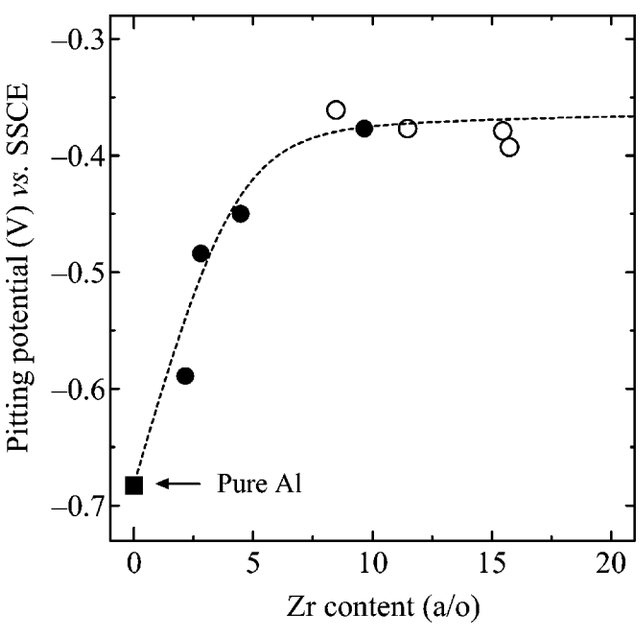

Figure 12. Pitting potentials as a function of composition for the Al-Zr alloys described in Fig. 11. Alloys electrodeposited from solutions containing (●) Zr(II) and (○) Zr(IV).

The rounded nodular structure that is often associated with amorphous deposits is not necessarily obtained in all the amorphous electrodeposits. Figure 10 shows the as-deposited surfaces of three alloys deposited at different current densities. Each contains 15.6-16.6 atom % Zr and has an identical amorphous XRD structure. The morphologies are quite different. Deposits formed at low current density ($\leqslant$10 mA cm^{-2}) are poorly nucleated and have a particulate or platelet morphology (see Fig. 10a and b). In contrast, the amorphous deposit formed at 20 mA cm^{-2} is dense and compact. To the naked eye, it also has a specular appearance. We believe that this may be due to a Zr^{3+} intermediate that may be more prevalent at the lower current densities, *i.e.*, at more positive deposition potentials. The limited solubility of Zr^{3+} may lead to its precipitation on the electrode surface and to disruption of Al-Zr alloy film growth.

Pitting potential measurements of Al-Zr alloys.—The corrosion resistance of the electrodeposited Al-Zr alloys was investigated by recording potentiodynamic anodic polarization curves in N_2-saturated aqueous 0.1 M NaCl. These polarization curves are shown in Fig. 11. As noted for Al-Mn alloys examined under similar conditions,[23] Al-Zr alloys display a stable passive region characterized by a very small potential-independent current followed by a sudden rise in current at the pitting potential as the deposit undergoes electrodissolution. The variation of the Al-Zr pitting potential with alloy composition is shown in Fig. 12. The addition of 8 atom % or more Zr increases the pitting potential of the alloy by about +0.3 V *vs.* pure Al. This increase is close to the value for the $Al_{97}Zr_3$ alloy that was prepared by sputter deposition.[48]

Acknowledgments

This research was supported by the Air Force Office of Scientific Research grant no. F49620-00-1-0123.

The University of Mississippi assisted in meeting the publication costs of this article.

References

1. T. B. Massalski, *Binary Alloy Phase Diagrams*, American Society of Metals, Metals Park, OH (1990).
2. L. M. Burov and A. A. Yakunin, *Russ. J. Phys. Chem.*, **42**, 540 (1968).
3. N. I. Varich, L. F. Kolomoytseva, A. N. Varich, and V. V. Maslov, *Fiz. Met. Metalloved.*, **27**, 361 (1969).
4. E. Sahin and H. Jones, in *Rapidly Quenched Metals III, Proceedings of the 3rd International Conference on Rapidly Quenched Metals*, Vol. 138, The Metals Society, London (1978).
5. Z. A. Chaudhury and C. Suryanarayana, *Metallography*, **17**, 231 (1984).
6. S. K. Pandey, D. K. Gangopadhyah, and C. Suryanarayana, *Z. Metallkd.*, **77**, 12 (1986).
7. Z. A. Chaudhury and C. Suryanarayana, *Mater. Sci. Eng.*, **67**, 47 (1984).
8. V. I. Dobatkin, V. I. Elagin, V. M. Fedorov, and R. M. Sizova, *Russ. Metall.*, **2**, 122 (1970).
9. N. Ryum, *Acta Metall.*, **17**, 269 (1969).
10. O. Izumi and D. Oelschlagel, *Scr. Metall.*, **3**, 619 (1969).
11. T. Ohashi and R. Ichikawa, *Metall. Trans.*, **3**, 2300 (1972).
12. E. Nes, *Acta Metall.*, **20**, 499 (1972).
13. E. Nes and H. Billdal, *Acta Metall.*, **25**, 1039 (1977).
14. E. Nes and H. Billdal, *Acta Metall.*, **25**, 1031 (1977).
15. G. W. Delamore and R. W. Smith, *Metall. Trans.*, **2**, 1733 (1971).
16. T. Ohashi and R. Ichikawa, *Z. Metallkd.*, **64**, 517 (1973).
17. R. Grimes, M. J. Stowell, and B. M. Watts, *Met. Technol. (London)*, **3**, 154 (1976).
18. B. M. Watts, M. J. Stowell, B. L. Baike, and D. G. E. Owen, *Met. Sci.*, **10**, 198 (1976).
19. B. M. Watts, M. J. Stowell, B. L. Baike, and D. G. E. Owen, *Met. Sci.*, **10**, 189 (1976).
20. T. P. Moffat, *J. Electrochem. Soc.*, **141**, L115 (1994).
21. M. R. Ali, A. Nishikata, and T. Tsuru, *Electrochim. Acta*, **42**, 2347 (1997).
22. G. R. Stafford, *J. Electrochem. Soc.*, **136**, 635 (1989).
23. T. P. Moffat, G. R. Stafford, and D. E. Hall, *J. Electrochem. Soc.*, **140**, 2779 (1993).
24. G. R. Stafford, *J. Electrochem. Soc.*, **141**, 245 (1994).
25. T. Tsuda, C. L. Hussey, G. R. Stafford, and J. E. Bonevich, *J. Electrochem. Soc.*, **150**, C234 (2003).
26. T. Tsuda and C. L. Hussey, *J. Min. Metall., B*, **39**, 3 (2003).
27. G. R. Stafford and C. L. Hussey, in *Advances in Electrochemical Science and Engineering*, Vol. 7, R. C. Alkire and D. M. Kolb, Editors, p. 275, Wiley-VCH Verlag GmbH, Weinheim, Germany (2002).
28. M. Kawase and Y. Ito, *J. Appl. Electrochem.*, **33**, 785 (2003).
29. B. Gilbert, G. Mamantov, and K. W. Fung, *Inorg. Chem.*, **14**, 1802 (1975).
30. M. Katabua, P. Rolland, G. Mamantov, and L. Hulett, *Inorg. Chem.*, **21**, 3569 (1982).
31. D. Sun and T. Hughbanks, *Inorg. Chem.*, **38**, 992 (1999).
32. R. Bilewicz, K. Wikiel, R. Osteryoung, and J. Osteryoung, *Anal. Chem.*, **61**, 965 (1989).
33. T. B. Scheffler and C. L. Hussey, *Inorg. Chem.*, **23**, 1926 (1984).
34. R. S. Nicholson, *Anal. Chem.*, **37**, 1406 (1965).
35. R. S. Nicholson and I. Shain, *Anal. Chem.*, **36**, 706 (1964).
36. A. A. Fannin, Jr., D. A. Floreani, L. A. King, J. S. Landers, B. J. Piersma, D. J. Stech, R. L. Vaughn, J. S. Wilkes, and L. Williams John, *J. Phys. Chem.*, **88**, 2614 (1984).
37. J. O'M. Bockris and A. K. N. Reddy, *Modern Electrochemistry*, Plenum Press, New York (1998).
38. R. T. Carlin, R. A. Osteryoung, J. S. Wilkes, and J. Rovang, *Inorg. Chem.*, **29**, 3003 (1990).
39. G. R. Stafford and T. P. Moffat, *J. Electrochem. Soc.*, **142**, 3288 (1995).
40. O. Ruff and R. Wallstein, *Z. Anorg. Allg. Chem.*, **128**, 96 (1923).
41. E. M. Larsen, J. W. Moyer, F. Gil-Arnao, and M. J. Camp, *Inorg. Chem.*, **13**, 574 (1974).
42. J. Brynestad, S. von Winbush, H. L. Yakel, and G. P. Smith, *Inorg. Nucl. Chem. Lett.*, **6**, 889 (1970).
43. K. W. Fung and G. Mamantov, *J. Electroanal. Chem. Interfacial Electrochem.*, **35**, 27 (1972).
44. L. W. Austin, M. G. Vucich, and E. J. Smith, *Electrochem. Technol.*, **1**, 267 (1963).
45. T. Tsuda, C. L. Hussey, G. R. Stafford, and J. E. Bonevich, *J. Electrochem. Soc.*, **151**, C379 (2004).
46. T. Takenaka and M. Kawakami, *Int. J. Mater. Product Tech.*, **2**, 500 (2001).
47. B. Grushko and G. R. Stafford, *Metall. Trans. A*, **20**, 1351 (1989).
48. G. D. Davis, W. C. Moshier, T. L. Fritz, and G. O. Cote, *J. Electrochem. Soc.*, **137**, 422 (1990).